Nanomedicine: Nanotechnology, Biology, and Medicine
26 (2020) 102174

nanomedicine
Nanotechnology, Biology, and Medicine

nanomedjournal.com

Thin graphene oxide nanoflakes modulate glutamatergic synapses in the amygdala cultured circuits: Exploiting synaptic approaches to anxiety disorders

Nicola Secomandi, PhD[a], Audrey Franceschi Biagioni, PhD[a], Kostas Kostarelos, PhD[b], Giada Cellot, PhD[a,*], Laura Ballerini, MD[a,*]

[a]*International School for Advanced Studies, SISSA, Trieste, Italy*

[b]*Nanomedicine Lab, Faculty of Biology, Medicine & Health and National Graphene Institute, AV Hill Building, University of Manchester, Manchester, United Kingdom*

Abstract

Anxiety disorders (ADs) are nervous system maladies involving changes in the amygdala synaptic circuitry, such as an upregulation of excitatory neurotransmission at glutamatergic synapses. In the field of nanotechnology, thin graphene oxide flakes with nanoscale lateral size (s-GO) have shown outstanding promise for the manipulation of excitatory neuronal transmission with high temporal and spatial precision, thus they were considered as ideal candidates for modulating amygdalar glutamatergic transmission. Here, we validated an *in vitro* model of amygdala circuitry as a screening tool to target synapses, towards development of future ADs treatments. After one week *in vitro*, dissociated amygdalar neurons reconnected forming functional networks, whose development recapitulated that of the tissue of origin. When acutely applied to these cultures, s-GO flakes induced a selective modification of excitatory activity. This type of interaction between s-GO and amygdalar neurons may form the basis for the exploitation of alternative approaches in the treatment of ADs.

Key words: Graphene oxide; Synapses; Amygdala; Nanoparticles; Glutamate; Anxiety disorders

Anxiety disorders (ADs), including phobias and post-traumatic stress disorder, comprise diseases whose common features are excessive and enduring fear, anxiety or avoidance to situations perceived as a threat by the subject.[1] These syndromes are the most prevalent type of psychiatric illness in western societies[2] and have a significant socio-economic burden.[3] Studies, both in patients and in animal models of ADs, have indicated that a potential mechanistic explanation for the behavioral expression of these syndromes, can be glutamate hyper-activity in excitatory synapses of the amygdala.[4–8]

Amygdaloid complex is an almond shaped small structure located deeply into the temporal lobes of the right and left hemispheres, whose function has been related to the processing of emotions, such as fear.[9] These structures are composed by clusters of nuclei, uniquely connected with other intra-amygdalar bodies or encephalic areas.[10] That specific wiring lies at the basis of amygdala functionality, which works as a processor receiving sensory and cognitive information from the thalamus and cortex and, upon elaboration of these inputs, sends diverse outputs to other brain structures, resulting in a range of behavioral/autonomic and endocrine responses to various environmental contests.[11] The characterization of this complex connectivity has been instrumental also in identifying dysfunctional pathways in ADs and new therapeutic approaches aimed at manipulating synaptic functions with a high spatial–temporal control. To address such demands, innovative and promising tools might emerge from nanotechnology developments.

Recently, thin and small (between 100 and 300 nm in lateral size) graphene oxide flake (s-GO), a type of carbon-based nanomaterial, has been found to interfere selectively with the activity of hippocampal glutamatergic synapses.[12,13] When delivered *in vivo* into the hippocampus of juvenile rats, this nanomaterial induced a selective, transient and spatially restricted modulation of the excitatory synaptic activity.[13] The

Funding: This work was supported by the European Union's Horizon 2020 research and innovation program under Grant Agreements 696656 and 785219 Graphene Flagship.

*Corresponding authors.

E-mail addresses: cellot@sissa.it (G. Cellot), laura.ballerini@sissa.it (L. Ballerini).

https://doi.org/10.1016/j.nano.2020.102174

ability of s-GO for high spatial and temporal precision in targeting glutamatergic synaptic transmission might be exploited to address the excitatory malfunction of the amygdala, underlying ADs. However, to date it is completely unexplored whether s-GO exerts effects on the activity of amygdalar neurons. The restricted anatomical access to amygdaloid bodies limits specific experimental synaptic studies *in vivo*, thus, more simplified models of amygdala circuitries are needed for fast screening of new drugs, molecules and nanomaterials that might have applications for the treatment of ADs.

In the current work, we developed an *in vitro* model of amygdalar neuronal networks, whose activity was explored by patch clamp recordings. We show that after one week *in vitro* neurons reconnected, forming active synapses, whose characteristics underwent to a process of maturation, resembling those occurring *in vivo*. The acute treatment with s-GO of these cultures strongly modulated glutamatergic signaling, indicating that the nanomaterial interacted with amygdalar neurons at the level of excitatory synapses. Thus, we validated this alternative *in vitro* model of amygdala for studying the effect of innovative nano-sized tools for the therapy of ADs.

Materials and methods

Graphene oxide nanosheet synthesis and characterization

Graphene oxide (GO) sheets of small lateral dimensions were synthesized using a modified Hummers method. All materials used were produced under endotoxin-free conditions, and yielded single to few-layer sheets with identical surface chemistry and thickness. The s-GO was constituted mostly of nanometer-sized sheets between 50 nm and 2 μm. A detailed description for the preparation and characterization of this nanomaterial can be found elsewhere.[12,13]

Dissociated amygdalar cultures

Isolation of rat brains was performed in agreement with the Italian law (decree 26/14) and the European Union (EU) guidelines (2007/526/CE and 2010/63/UE) and all the procedures were authorized by the local veterinary authorities and by the institutional (ISAS) ethical committee. The animal use was approved by the Italian Ministry of Health.

Primary cultures of amygdalar cells were obtained from Wistar rats aged 8-10 days. Brains were quickly removed from the skull and placed in fresh ice-cold artificial cerebrospinal fluid (ACSF) whose composition was (in mM): 124 NaCl, 24 $NaHCO_3$, 13 glucose, 5 HEPES, 2.5 KCl, 2 $CaCl_2$, 2 $MgSO_4$ and 1,2 $NaPO_4H_2$ with a pH of 7.3-7.4 when saturated with 95% O_2 and 5% CO_2.[14]

Coronal brain slices (400 μm) including the amygdala complex were cut using a vibratome (Leica VT100S) and transferred into a dish containing ice-cold oxygenated ACSF. Under a dissecting microscope (Olympus SZ40), the regions containing the amygdalar nuclei were isolated using a biopsy punch with a diameter of 1 mm (Kai Medical, Japan). The collected tissue was enzymatically and mechanically dissociated following standard protocol.[15] Cells were seeded onto poly-L-ornithine-coated glass coverslips at a density of 800 cells/mm^2 and maintained in controlled conditions (at 37 °C, 5% CO2) for 8-12 days.

Immunofluorescence

Cultures were fixed after 8 or 12 days *in vitro* (DIV) with 4% paraformaldehyde in PBS for 20 min and adding 1% glutaraldehyde in PBS for 1 h for GABA staining as previously reported.[16] Cells were permeabilized with Triton X-100 (0.3%), incubated for 30 min at room temperature (RT) with primary antibodies and, after being rinsed with PBS, incubated with secondary antibodies for 30 min at RT. As primary antibodies, we used mouse monoclonal anti-GFAP antibody (Sigma G3893, 1:500 dilution) and rabbit polyclonal anti- β-tubulin III antibody (Sigma T2200, 1:500 dilution) to label glial cells and neurons respectively.[12] GABAergic neurons were co-stained with mouse monoclonal anti- β-tubulin III antibody (Sigma T8535, 1:500 dilution) and anti-GABA polyclonal antibody produced in rabbit (Sigma A2052, 1:300 dilution[17]). As secondary antibodies, we employed Alexa 594 goat anti-rabbit (Invitrogen, 1:500 dilution), Alexa 594 goat anti-mouse (Invitrogen, 1:500 dilution), Alexa 488 goat anti-mouse (Invitrogen, 1:500 dilution) and Alexa 488 goat anti-rabbit (Invitrogen, 1:500 dilution). Nuclei were marked with DAPI (1:400, Invitrogen). For each sample, images of 5 randomly selected fields were acquired using a confocal microscope (Nikon Eclipse Ti, Nikon, Japan). Images from three different culture series were analyzed with the software ImageJ (NIH).

Electrophysiology

Patch clamp whole-cell recordings were performed from neurons using glass micropipettes with a resistance of 4÷7 MΩ when filled with the intracellular saline solution composed of (mM): 120 K gluconate, 20 KCl, 10 HEPES, 10 EGTA, 2 $MgCl_2$, 2 Na_2ATP, pH 7.3 and osmolarity 300 mOsm. All experiments were performed at room temperature from cells continuously perfused at 5 ml/min with the standard extracellular solution containing (mM): 150 NaCl, 4 KCl, 2 $CaCl_2$, 1 $MgCl_2$, 10 HEPES, 10 glucose, pH 7.4. All data were recorded by means of a Multiclamp 700B patch amplifier (Axon CNS, Molecular Devices) digitized at 10 kHz by pClamp 10 software (Molecular Devices LLC, USA). Input resistance and cells capacitance were measured online with the membrane test feature of the pClamp software. Spontaneous activity was recorded in voltage clamp mode at a holding potential of −56 mV (not corrected for the liquid junction potential which was −14 mV).

Spontaneous postsynaptic currents (PSCs) were analyzed offline using the software AxoGraph X (Axograph Scientific), which exploits a detection algorithm based on a sliding template. For each recording, all the collected events were averaged and the peak amplitude and kinetic properties of the mean current were calculated. The decay time of PSCs was calculated by fitting the decaying phase of the current with a mono-exponential function. Templates characterized by diverse decay times were used to separate offline glutamate AMPA-receptor mediated

PSCs (~3 ms) and those mediated by $GABA_A$ receptors (~20 ms).

Pairs of monosynaptically connected neurons, in which the cells were apart ~100 μm one from the other, were recognized by the short latency 2.9 ± 0.3 ms[12,18] between the peak of the presynaptic neuron and the onset of the evoked PSC (ePSC). Using a Picospritzer (PDES-02DX; NPI electronic GmbH, Germany), an injection of pressurized air (500 ms, 0.5 PSI) was exploited to deliver a puff of s-GO to the amygdalar neurons. The puff pipette was filled with standard saline solution (control) or with s-GO (100 μg/ml diluted in saline solution) and located at a distance of about 200 μm from the recorded cell. Considering 1 ml of extracellular solutions in our recording chamber, we estimated that the concentration of s-GO reaching the patch-clamped neurons was at least 10% of that present in the puff pipette as previously reported.[12,13] PSCs were recorded before (10 min, baseline) and after (5 min) the local ejection.

Statistical analysis

All values from samples subjected to the same experimental protocols were pooled together and expressed as mean ± S.E.M. with n = number of neurons, if not otherwise indicated. D'Agostino & Pearson omnibus normality test was applied to evaluate the statistical distribution of the data sets. Statistically significant difference between two data sets was assessed by Student's t test or by Mann–Whitney test. Statistical significance was determined at $P < 0.05$.

Results

To explore the impact of nanomaterials on amygdalar circuitry, in particular on subcellular components, such as synapses, we developed a simplified *in vitro* model of amygdala. This structure was isolated with a high degree of precision from coronal brain slices using a biopsy punch. The collected region underwent a process of enzymatic digestion (see Materials and Methods); then cells were seeded on peptide-covered glass coverslips and allowed to develop for 8-12 DIV. In parallel, the slices from which the amygdalar complexes were isolated were processed with Nissl staining, to assess brain structures and confirm the correct anatomical sampling of amygdalae (Figure 1, *A*).

The maturation of amygdalar cultures *in vitro* was characterized through immunofluorescence technique and confocal microscopy. Fixed preparations were immunostained for neuronal and glial markers at two different time points of their development (8 and 12 DIV) to measure culture size and cell composition (Figure 1, *B-E*). Neurons were labeled with antibodies against the specific cytoskeletal components β-tubulin III (in red) and against glial fibrillary acidic protein (GFAP, in green) to visualize glial cells. Nuclei were marked with DAPI (in blue). As shown by the z-stack reconstructions in Figure 1, *B*, glial cell density remained stable between 8 and 12 DIV (at 8 DIV: 110.6 ± 7.8 cells/mm^2 and at 12 DIV: 98.0 ± 5.3 GFAP positive cells/mm^2; n = 30 visual fields each condition), while neuronal density decreased along with the culture aging (at 8 DIV: 80.3 ± 4.8 cells/mm^2 and at 12 DIV: 64.2 ± 4.3 cells/mm^2; P = 0.0131, Figure 1, *B-C*). We further explored the neuronal composition of our cultures by determining the amount of inhibitory neurons. To this aim, we co-immunostained cells with antibodies against β-tubulin III (in red) and GABA (in light blue, Figure 1, *D*).

The amount of double positive cells, identified as GABAergic neurons, was not changed between 8 and 12 DIV (42% and 40% respectively, n = 30 visual fields for each conditions, Figure 1, *E*). Thus, dissociated amygdalar cultures appeared healthy and formed by well-differentiated GFAP-positive cells and different neuronal phenotypes. Their composition appeared stable over time with the exception of a slight, but statistically significant reduction in the number of neurons in older cultures.

Next, we tested amygdalar circuit activity *in vitro* by patch clamp recording of basal synaptic activity (voltage clamp mode) from single cells which were used as probes to sense inputs received by surrounding neurons. Figure 1, *F* shows exemplificative recordings from neurons at 8 and 12 DIV, in which the current deflections correspond to spontaneous PSCs (sPSCs). sPSCs frequencies were slightly larger, although not significantly, in older cultures (8 DIV: 1.5 ± 0.3 Hz, n = 21; 12 DIV: 2.4 ± 0.4 Hz, n = 41; Figure 1, *G*), while PSCs amplitudes increased in older cultures (from 20 ± 1 pA 8 DIV to 30 ± 2 pA 12 DIV; Figure 1, *H*). Such statistically significant difference (P = 0.0003) is in agreement with the presence of more mature synapses at the end of the second week *in vitro*.

In amygdalar cultures, spontaneous synaptic activity was composed by a mixed population of fast (~3 ms) and slow (~20 ms) decaying sPSCs. The former were abolished by the application of CNQX (10 μM), an antagonist of glutamate AMPA receptor mediated currents (n = 6), while the latter were blocked by treatment with gabazine (10 μM), a $GABA_A$ receptor antagonist (n = 3). Their kinetic properties together with their pharmacology support their excitatory glutamatergic (EPSCs; fast decaying events) or inhibitory GABAergic (IPSCs; slow decaying events) nature.

The diverse decay times of EPSCs and IPSCs were exploited to isolate them offline (see methods). Figure 2, *A* displays examples of fast decaying excitatory and slow decaying inhibitory sPSCs, collected from the traces of Figure 1, *F*. The analysis of the EPSCs and IPSCs revealed small changes in their frequencies during the maturation of the cultures (EPSCs from 1.1 ± 0.3 Hz to 2.1 ± 0.4 Hz; IPSCs from 0.4 ± 0.1 Hz to 0.3 ± 0.1 Hz, 8 and 12 DIV, respectively; Figure 2, *B*). However, the amplitudes of both EPSCs and IPSCs were enhanced in a statistically significant manner in older cultures in respect to younger ones (EPSCs from 17 ± 1 pA to 22 ± 1 pA, 8 and 12 DIV, respectively P = 0.008; IPSCs: from 25 ± 3 pA to 39 ± 3 pA, 8 and 12 DIV, respectively, P = 0.005; Figure 2, *C*). When analyzing the kinetic properties of IPSCs and EPSCs separately, we found that the rise and decay times of EPSCs both increased during neuronal growth (rise time: from 0.72 ± 0.02 ms to 1.02 ± 0.04 ms, from 8 and 12 DIV, respectively, $P < 0.0001$; decay time: from 2.64 ± 0.16 ms to 3.64 ± 0.18 ms, 8 and 12 DIV, respectively, P = 0.0042). Conversely, while also the IPSCs rise time became longer (from 1.37 ± 0.07 ms to 2.05 ± 0.05 ms, 8 and 12 DIV, $P < 0.0001$), their decay time were faster in older cells (from 21.10 ± 1.31 ms to 17.31 ± 0.88 ms, 8 and 12 DIV, $P < 0.0001$; Figure 2, *D*). All together these findings indicated that both the excitatory and

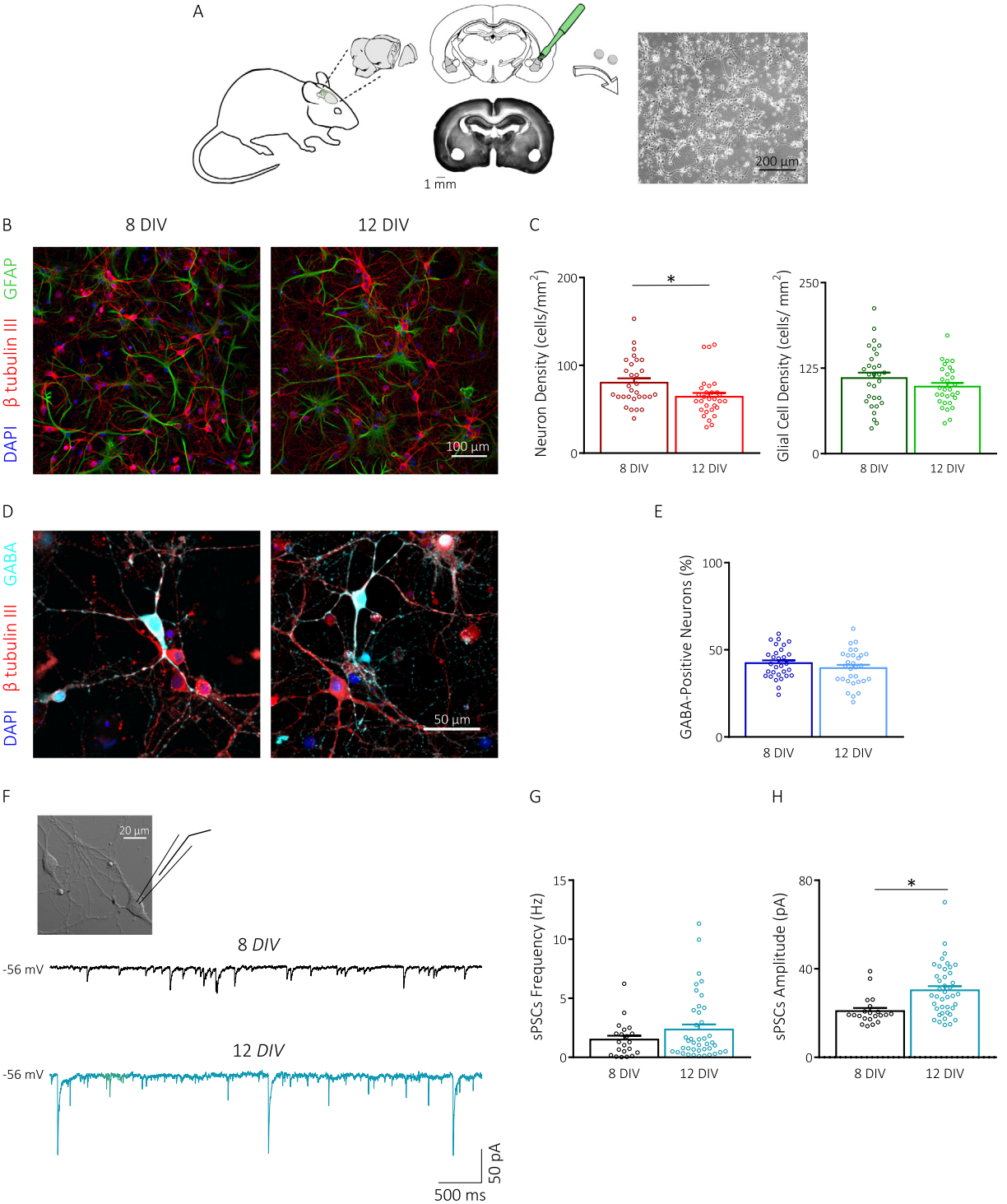

Figure 1. Dissociated amygdalar neurons reconstruct functional networks *in vitro*. **(A)** Schematic representation of dissociated amygdalar culture procedure: brains isolated from juvenile rats are sliced (left); amygdaloid nuclei are precisely isolated by a biopsy punch (in green) and enzymatically dissociated to get pure cultures (right). The remaining tissue is stained with Nissl procedure (middle) to confirm the sampling of the amygdalae. **(B)** Confocal images of cultures at 8 (left) and 12 (right) DIV, stained with β tubulin III (in red), GFAP (in green) and DAPI for nuclei (in blue). **(C)** Bar plots summarizing the neuron (left) and glial (right) cell densities at 8 and 12 DIV. Note the decrease in neuronal density in cultures at 12 DIV. **(D)** Confocal images of neurons double stained with β tubulin III (in red) and GABA (in light blue) at 8 and 12 DIV. **(E)** Bar plots summarize the percentage of GABAergic neurons (double-positive cells) at the two time points. **(F)**. On the top, representation of patch clamp recording from single cell. Below, exemplificative traces of spontaneous network activity recorded from amygdalar neurons after 8 and 12 DIV. Bar plots showing the frequency **(G)** and the amplitude **(H)** of sPSCs at 8 and 12 DIV.In all bar plots, dots superimposed to the bars are single values and * $P < 0.05$.

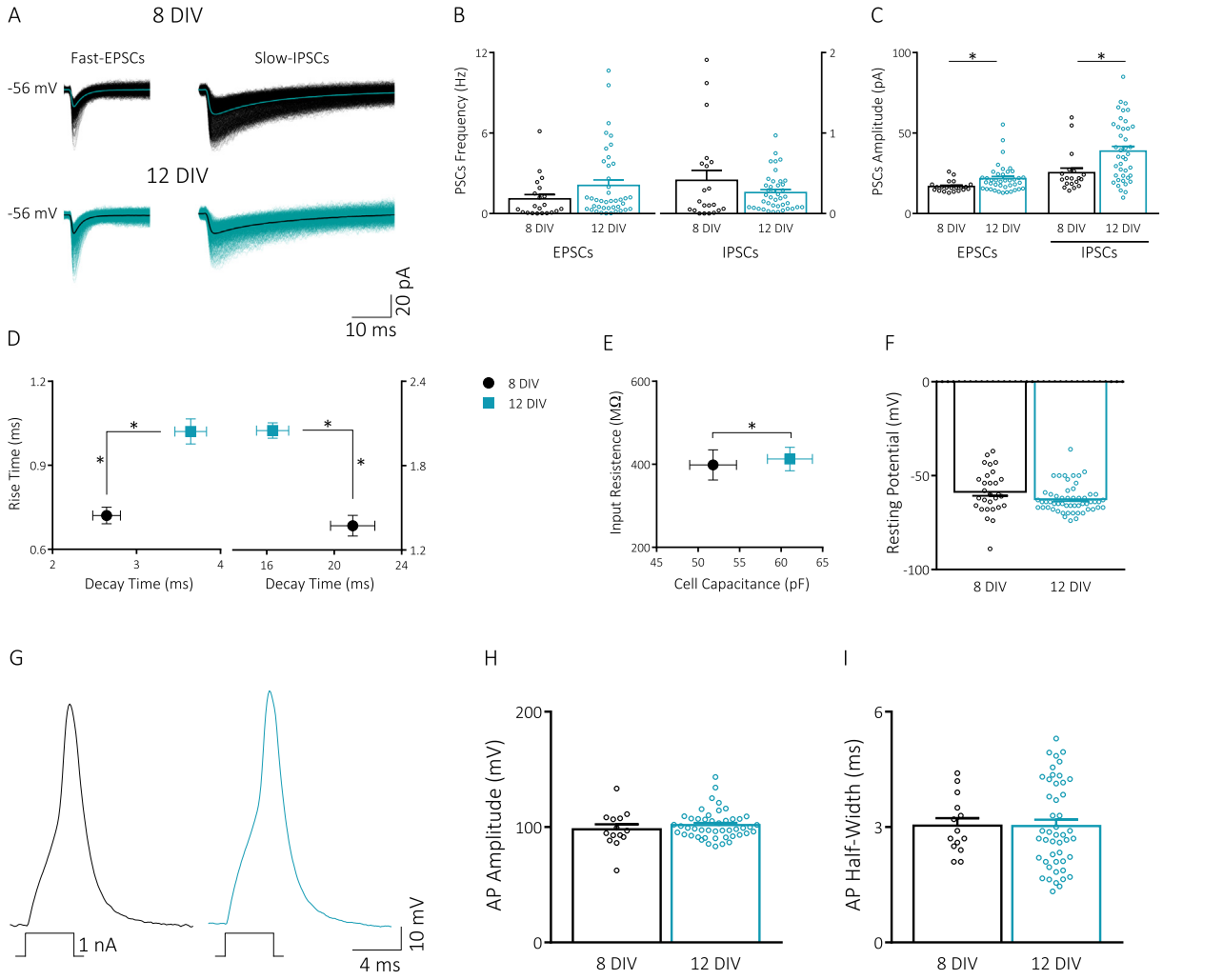

Figure 2. Electrophysiological characterization of amygdalar neurons. **(A)** Offline PSCs analysis of fast-EPSCs (left) and slow-IPSCs (right) at 8 and 12 DIV. Bar plots showing the frequencies **(B)** and the amplitudes **(C)** of EPSCs and IPSCs at the two considered temporal points. The amplitudes of both the types of currents are increased in more mature cultures. **(D)** Summary graphs of EPSC and IPSC kinetic properties at 8 (black circle) and 12 (blue square) DIV. **(E)** Summary graph of input resistance and cell capacitance at 8 (black circle) and 12 (blue square) DIV. Capacitance becomes larger in more mature neurons. **(F)** Bar plots summarizing the neuronal resting membrane potential at the two temporal points. **(G)** Representative traces of action potentials in neurons at 8 (black) and 12 (blue) DIV neurons, elicited by current injection (the protocol is shown below). Bar plots summarizing the AP amplitudes **(H)** and half-width **(I)** in the two conditions In all bar plots dots superimposed to the bars are single values and * $P < 0.05$.

inhibitory components of the network mature during the second week of differentiation *in vitro*.

With the exception of IPSCs decay time, all sPSCs kinetic parameters slowed down during neuronal growth, a result in accordance with an increase in the electrotonic filtering of neurites (*e.g.* longer neurites), following dimensional growth of single neurons. Indeed, cell capacitance, an indirect measure of neuronal size,[19] of more mature neurons was increased in respect to younger cultures (from 52 ± 3 pF to 61 ± 3 pF, $n = 30$ and $n = 55$, 8 and 12 DIV respectively, $P = 0.031$), while the input resistance (from 398 ± 36 MΩ to 413 ± 28 MΩ, 8 and 12 DIV, Figure 2, *E*) and the resting membrane potential (from −59 ± 2 mV to −63 ± 1 mV, 8 and 12 DIV, Figure 2, *F*) were similar at the two time points measured.

In a further set of experiments, we induced in current clamp mode action potentials (APs) by injecting neurons with short square pulses of depolarizing currents (Figure 2, *G*). The analysis of AP amplitudes (at 8 DIV: 98 ± 4 mV, $n = 14$, and 12 DIV: 102 ± 2 mV, $n = 47$) and half-widths (at 8 DIV: 3.0 ± 0.2 ms 12 DIV: 3.0 ± 0.2 ms) detected no differences between the two culture groups (Figure 2, *G-I*), suggesting that APs were already mature after one week of growth *in vitro*.

We further investigated synaptic connectivity at 12 DIV by dual patch clamp recordings from pairs of mono-synaptically connected neurons (Figure 3, *A*): the presynaptic cell was elicited to fire APs in current clamp configuration, while the postsynaptic one was simultaneously clamped at −56 mV to monitor the presence of an ePSC (Figure 3, *B*, see methods). The probability to find monosynaptically connected pairs of neurons was high (75%, $n = 36$ pairs, Figure 3, *C*), indicating an elevated degree of connectivity in the neuronal network. In addition, the analysis of ePSCs kinetic features revealed that the majority (93%, $n = 29$, Figure 3, *D*) of

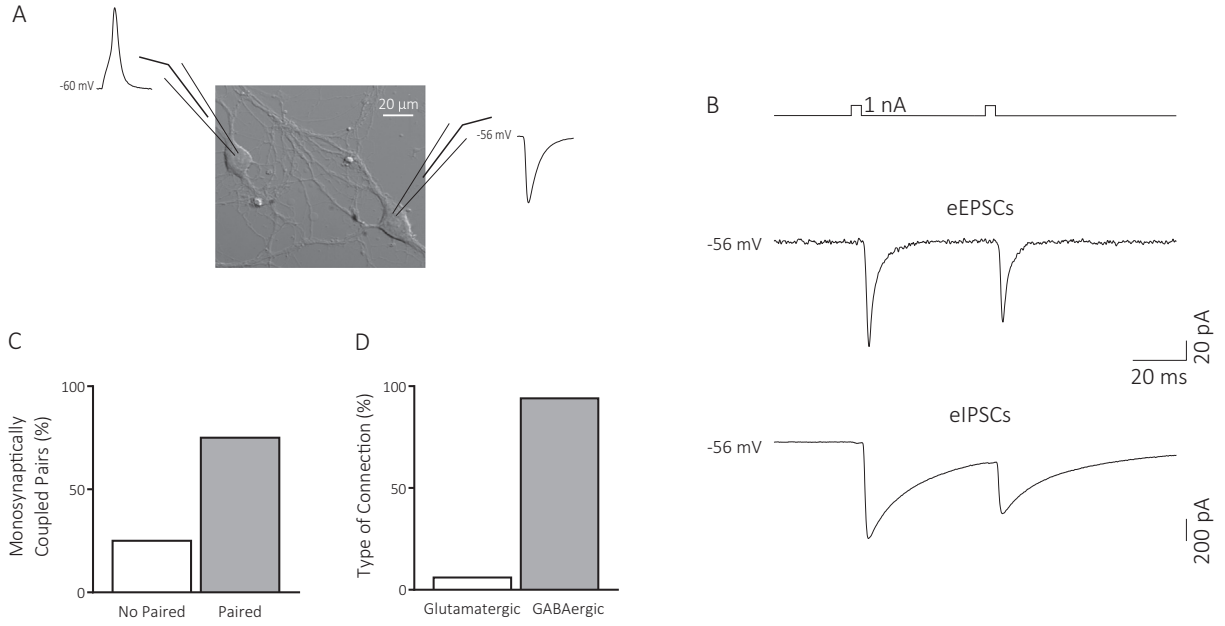

Figure 3. Electrophysiological characterization of unitary postsynaptic currents at 12 DIV. **(A)** Sketch of the experimental setting for pair recordings. **(B)** Currents injections (above, 4 ms, 1 nA@20 Hz) elicit action potentials in the presynaptic neuron (middle). Below, representative averaged traces of evoked unitary EPSCs or IPSCs recorded from postsynaptic neurons. **(C)** Bar plot summarizing the percentage of monosynaptically coupled pairs at 12 DIV. **(D)** Histograms showing the percentage of different type of connections in monosynaptically coupled pairs.

synapses activated slow decaying currents (~ 20 ms), identifiable as $GABA_A$ mediated IPSCs, while only a subset of these (7%) showed fast ePSCs (~3 ms), compatible with AMPA receptor mediated EPSCs (Figure 3, *B*). The short-term plasticity of these synapses, evaluated by a pair of stimuli at 20 Hz (see methods), revealed that both excitatory and inhibitory connections underwent to short-term depression of ePSCs (ratios between the amplitude of the second and first ePSCs were 0.9 ± 0.1 for the excitatory connections and 0.7 ± 0.1 for the inhibitory ones; Figure 3, *B*).

Overall, our electrophysiological characterization showed that after 8 DIV, dissociated amygdalar neurons reconnected forming functional synapses, whose activity was further modified during the second week of development *in vitro*, compatibly with the acquisition of a more mature phenotype of the culture. We decided to exploit such simplified model to test the interaction of s-GO with amygdalar neurons.

In the last set of experiments, we tested whether s-GO affected synaptic activity as showed before for hippocampal culture.[12,13] In mature cultures (12 DIV), a puff of solution containing s-GO (or saline as control) was pressure-applied through a pipette located at a distance of 200 µm from a neuron, while its spontaneous activity was monitored in voltage clamp mode (Figure 4, *A*). Figure 4, *B* shows that s-GO application (orange arrow) produced a change in neuronal activity, while the treatment with saline (black arrow) exerted no effect. Magnifications of the traces before and after the puffs (insets in the bottom row of Figure 4, *B*) display that s-GO induced changes in the frequency but not in the amplitude of sPSCs. A quantification of these parameters detected a statistically significant increment in the after puffs frequencies of sPSCs between saline (n = 12) and s-GO (n = 12) treated neurons (for saline-treated: 2.5 ± 0.5 Hz and for s-GO-treated: 5.5 ± 1.1 Hz, P = 0.0447; Figure 4, *C*), while the pre-puffs frequencies were similar between the two treatments (for saline-treated: 2.6 ± 0.5 Hz and for s-GO-treated: 4.2 ± 1.0 Hz; Figure 4, *C*). No changes were detected in the amplitudes of sPSCs due to s-GO application (pre-puff values were 65 ± 16 pA for saline and 66 ± 13 pA for s-GO; post-puff values were 57 ± 13 pA for saline and 48 ± 6 pA for s-GO; Figure 4, *D*).

To better point out the effect of s-GO, we normalized the post-puff values for the pre-puff ones for each cell (Figure 4, *E*). Thus, we observed a change of 78.8% ± 36.5% in sPSCs frequency after the puff in s-GO treated neurons (P = 0.0424); on the opposite in saline treated cells this difference was not statistically relevant (−1.5% ± 5.0%; Figure 4, *E*). By isolating the excitatory and the inhibitory components of the network by means of offline analysis, we detected that s-GO induced modifications only in the frequency of EPSCs (for saline treated neurons: −0.4% ± 7.3%, and for s-GO treated ones: 130% ± 65.3%, P = 0.0255 pre *vs* post in s-GO treated samples; P = 0.0292 saline *vs* s-GO; Figure 4, *F*), while that of IPSCs was unchanged (12.1% ± 14.3%, for saline treated and 15.2% ± 19.5%, for s-GO treated; Figure 4, *G*). These results showed that this nanomaterial was able to interfere with the function of amygdalar neurons, by upregulating specifically the activity of excitatory synapses.

Discussion

In the current work, we studied the interaction of thin s-GO flakes with amygdalar neurons, showing that this material can modulate selectively the excitatory glutamatergic transmission in neuronal circuits obtained from that brain region. We developed

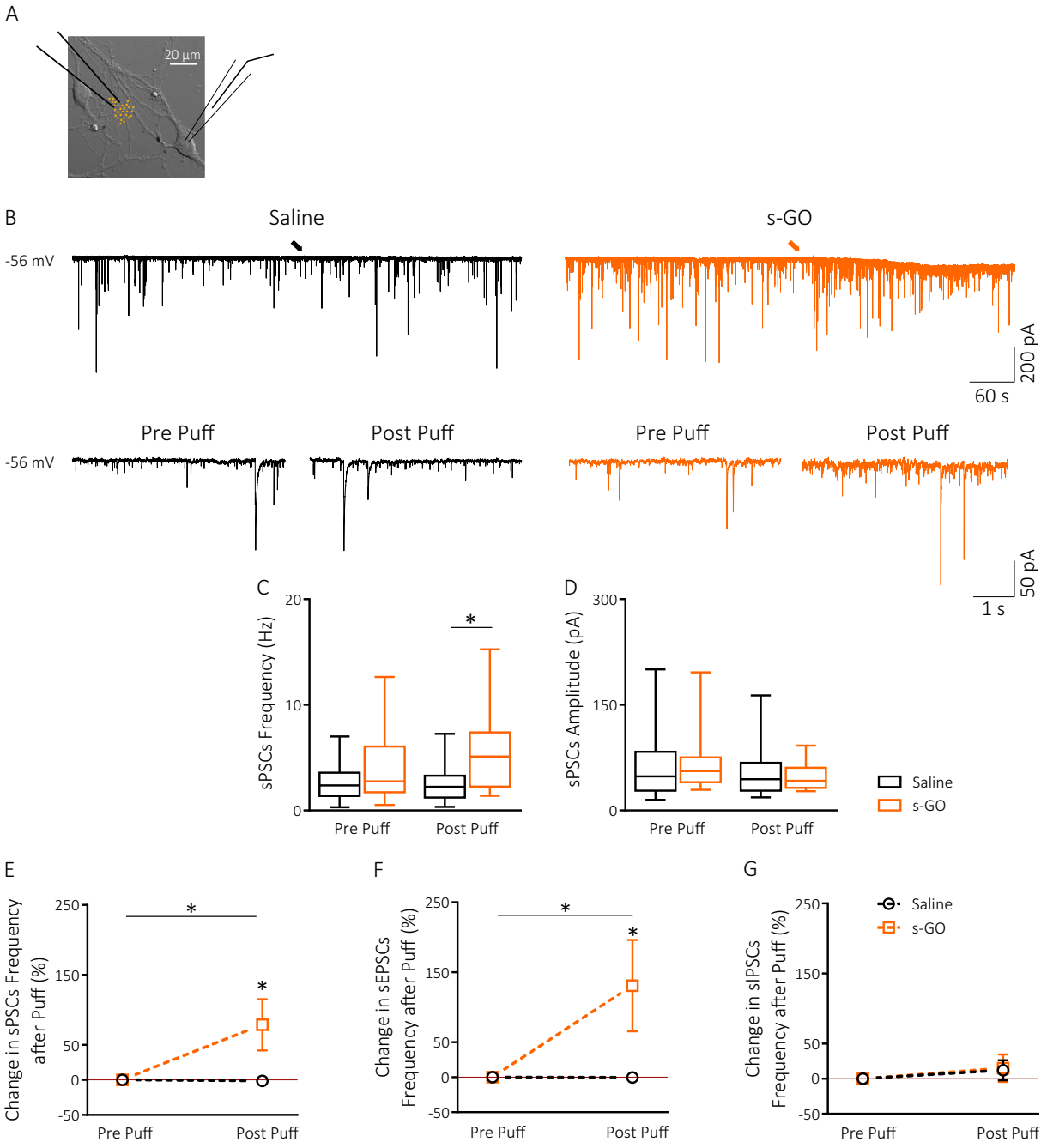

Figure 4. Acute application of s-GO interferes with glutamatergic activity of amygdalar neurons. **(A)** Sketch of the experimental setting. **(B)** Top, representative traces of the spontaneous synaptic activity during acute application of saline (left) or s-GO (right). Arrows represent the puff ejection (see methods). Bottom, magnified traces of the spontaneous synaptic activity recorded before and after saline (left) and s-GO (right) applications. Box plots summarize the sPSC frequency **(C)** and amplitude **(D)** before and after the acute application of saline (black) and s-GO (orange). sPSCs frequency is increased only by treatment with s-GO. Summary graphs of the change in sPSCs **(E)**, sEPSCs **(F)** and sIPSCs **(G)** frequency after the saline (black circle) and s-GO (orange square) puff. s-GO affects selectively the frequency of EPSCs. * $P < 0.05$.

dissociated cultures from the amygdalae to better dissect synaptic activity at the single cell level.[20,21] With respect to previous works,[14,22–25] we improved our preparation in terms of purity, due to a more precise procedure to explant amygdalae, confirmed by our Nissl staining. Cultured amygdalar circuits developed with a slight decrease in neurons during the second week *in vitro*, commonly observed in culture,[26] possibly related to a reduced availability of neurotrophic factors in respect to the *in vivo* condition.[27–29] However, despite the slight decline in the number of neurons, synaptic circuits seems to mature progressively, as indicated by the enhancement in the amplitude of both EPSCs and IPSCs at 12 DIV.

Also, the kinetic properties of sPSCs changed during this time window: rise times of EPSCs and IPSCs slowed down, while decay times got slower for EPSCs and faster for IPSCs. These trends match with those observed in amygdala explants obtained from animals at different ages,[30] indicating that in our model, neurons retraced a process of physiological maturation. While the speed-up of IPSCs decay time is compatible with a developmental switch from the α2- to the α1-subunit of $GABA_A$ receptors,[31] the slowing down of the other kinetic properties may be in part related to electrotonic filtering due to the growth of neurons during the maturation. Longer dendrites, indeed, would result in slower kinetic properties of sPSCs.[32] In agreement with this hypothesis, an increase in cell capacitance, an indicator of neuronal dimension, was observed at 12 DIV.[19] Conversely, we did not detect changes either in the properties of APs or in the resting membrane potentials, both reported similar to those of juvenile amygdalar neurons *in vivo*.[33] This confirms that our cultures present characteristics of mature amygdalar cells, with synapses undergoing a progressive strengthening when re-constructing active contacts *in vitro*.[34,35]

The latter observation was reinforced by the high connectivity detected by dual patch clamp recordings at 12 DIV: to note, the large majority of synaptic connections were GABAergic. This might appear controversial respect to the characterization of spontaneous network activity, where the frequency of EPSCs was prevalent when compared to that of IPSCs. The higher probability to find inhibitory synapses was possibly related to our experimental setting (dual recordings from neurons apart 100 μm one to the other), which would favor the selection of interneurons.[15]

The contribution of amygdala in shaping behavioral responses to environmental stimuli is developmentally regulated,[36,37] with complex fear responses consolidating around the third postnatal week.[38–40] Our electrophysiological characterization showed that, when the tissue of origin is collected from juvenile animals (P8-P10) and cells are allowed to differentiate *in vitro* for 8-12 days, cultures have single cell and synaptic features resembling those of *in vivo* amygdalar neurons of adolescent animals. Thus, we developed an easily accessible, simplified model of mature amygdala for the study of neuronal circuits, suited for fast screening of new drugs/materials/devices.

We used this system to show that s-GO could modify the synaptic function of amygdalar neurons. In fact, we reported that when acutely applied, the nanomaterial induced an enhancement in network activity, measured as an increase in the frequency of sPSCs in comparison to the pre-treatment baseline. Such effect was selective for the glutamatergic synapses, since s-GO changed the occurrence of EPSCs, but not that of IPSCs. s-GO exerts its effect modifying the presynaptic release of the neurotransmitter.[12,13] In other brain regions, the prolonged exposure to this nanomaterial resulted in the depletion of glutamate from presynaptic terminals, responsible for a decrease in the activity of excitatory synapses.[12,13] Since ADs are characterized by a glutamate mediated hyper-function of the amygdala,[4,7,41,42] s-GO might be exploited as therapeutics for long term impairing of glutamate release, ultimately down-regulating specifically this pathologically potentiated excitatory signaling.

Further experiments will be required to demonstrate that the increase in EPSC frequency reported here after s-GO application is only a transient effect and that, upon prolonged application, the nanomaterial is effective in reducing amygdalar activity. If the high spatial and temporal precision demonstrated by s-GO in downregulating excitatory signaling in other brain regions will be preserved in the amygdala, this nanomaterial might be a powerful alternative tool for the modulation of selective glutamatergic circuits whose activity is aberrant in ADs.

References

1. American Psychiatric Association APA. *Diagnostic and statistical manual of mental disorders: DSM-5*. 5th ed. Washington, D.C: American Psychiatric Association; 2013.
2. Kessler RC, Berglund P, Demler O, Jin R, Merikangas KR, Walters EE. Lifetime prevalence and age-of-onset distributions of DSM-IV disorders in the National Comorbidity Survey Replication. *Arch Gen Psychiatry* 2005;**62**:593.
3. Trautmann S, Rehm J, Wittchen H. The economic costs of mental disorders: do our societies react appropriately to the burden of mental disorders? *EMBO Rep* 2016;**17**:1245-9.
4. Cortese BM, Phan KL. The role of glutamate in anxiety and related disorders. *CNS Spectr* 2005;**10**:820-30.
5. Ganella DE, Kim JH. Developmental rodent models of fear and anxiety: from neurobiology to pharmacology: pharmacological studies in developmental anxiety. *Br J Pharmacol* 2014;**171**:4556-74.
6. Shin LM, Liberzon I. The neurocircuitry of fear, stress, and anxiety disorders. *Neuropsychopharmacology* 2010;**35**:169-91.
7. Wierońska J, Stachowicz K, Nowak G, Pilc A. The loss of glutamate-GABA harmony in anxiety disorders. In: Kalinin V (ed). *Anxiety disorders*. InTech, 2011.
8. Forster G, Andrew M, L. L, J. M. The role of the amygdala in anxiety disorders. In: Ferry B (ed). *The amygdala — a discrete multitasking manager*. InTech, 2012.
9. Aggleton JP. *The amygdala*. New York: A functional analysis. Second edition. Oxford Univ. Press; 2000.
10. Pitkänen A. Connectivity of the rat amygdaloid complex. In: *The amygdala. A functional analysis*. Oxford Univ. Press: New York, 2000, pp 31–115.
11. Yaniv D, Desmedt A, JaffAD R, Richter-Levin G. The amygdala and appraisal processes: stimulus and response complexity as an organizing factor. *Brain Res Rev* 2004;**44**:179-86.
12. Rauti R, Lozano N, León V, Scaini D, Musto M, Rago I, et al. Graphene oxide nanosheets reshape synaptic function in cultured brain networks. *ACS Nano* 2016;**10**:4459-71.
13. Rauti R, Medelin M, Newman L, Vranic S, Reina G, Bianco A, et al. Graphene oxide flakes tune excitatory neurotransmission in vivo by targeting hippocampal synapses. *Nano Lett* 2019;**19**:2858-70.
14. Wu YE, Pan L, Zuo Y, Li X, Hong W. Detecting activated cell populations using single-cell RNA-Seq. *Neuron* 2017; **96**: 313–329.e6.
15. Cellot G, Toma FM, Kasap Varley Z, Laishram J, Villari A, Quintana M, et al. Carbon nanotube scaffolds tune synaptic strength in cultured neural circuits: novel frontiers in nanomaterial-tissue interactions. *J Neurosci* 2011;**31**:12945-53.
16. Furlan F, Taccola G, Grandolfo M, Guasti L, Arcangeli A, Nistri A, et al. ERG conductance expression modulates the excitability of ventral horn GABAergic interneurons that control rhythmic oscillations in the developing mouse spinal cord. *J Neurosci* 2007;**27**:919-28.
17. Pampaloni NP, Lottner M, Giugliano M, Matruglio A, D'Amico F, Prato M, et al. Single-layer graphene modulates neuronal communication and augments membrane ion currents. *Nat Nanotechnol* 2018;**13**:755-64.

18. Pavlidis P, Montgomery J, Madison DV. Presynaptic protein kinase activity supports long-term potentiation at synapses between individual hippocampal neurons. *J Neurosci* 2000;**20**:4497-505.
19. Lindau M, Neher E. Patch-clamp techniques for time-resolved capacitance measurements in single cells. *Pflügers Arch Eur J Physiol* 1988;**411**:137-46.
20. Buchhalter JR, Dichter MA. Electrophysiological comparison of pyramidal and stellate nonpyramidal neurons in dissociated cell culture of rat hippocampus. *Brain Res Bull* 1991;**26**:333-8.
21. Godfrey EW, Nelson PG, Schrier BK, Breuer AC, Ransom BR. Neurons from fetal rat brain in a new cell culture system: a multidisciplinary analysis. *Brain Res* 1975;**90**:1-21.
22. Kasckow JW, Regmi A, Gill PS, Parkes DG, Geracioti TD. Regulation of corticotropin-releasing factor (CRF) messenger ribonucleic acid and CRF peptide in the amygdala: studies in primary amygdalar cultures. *Endocrinology* 1997;**138**:4774-82.
23. Lin CH, Huang YC, Tsai JJ, Gean PW. Modulation of voltage-dependent calcium currents by serotonin in acutely isolated rat amygdala neurons. *Synapse* 2001;**41**:351-9.
24. Lorenzo A, Díaz H, Carrer H, Cáceres A. Amygdala neurons in vitro: neurite growth and effects of estradiol: amygdaline neurite growth in vitro. *J Neurosci Res* 1992;**33**:418-35.
25. Mou L, Heldt SA, Ressler KJ. Rapid brain-derived neurotrophic factor-dependent sequestration of amygdala and hippocampal GABAA receptors via different tyrosine receptor kinase B-mediated phosphorylation pathways. *Neuroscience* 2011;**176**:72-85.
26. Ichikawa M, Muramoto K, Kobayashi K, Kawahara M, Kuroda Y. Formation and maturation of synapses in primary cultures of rat cerebral cortical cells: an electron microscopic study. *Neurosci Res* 1993;**16**:95-103.
27. Hanson MG, Shen S, Wiemelt AP, McMorris FA, Barres BA. Cyclic AMP Elevation is sufficient to promote the survival of spinal motor neurons *in vitro*. J Neurosci 1998; 18: 7361–7371.
28. Morrison RS, Sharma A, de Vellis J, Bradshaw RA. Basic fibroblast growth factor supports the survival of cerebral cortical neurons in primary culture. *Proc Natl Acad Sci* 1986;**83**:7537-41.
29. Walicke P, Cowan WM, Ueno N, Baird A, Guillemin R. Fibroblast growth factor promotes survival of dissociated hippocampal neurons and enhances neurite extension. *Proc Natl Acad Sci* 1986;**83**:3012-6.
30. Bosch D, Ehrlich I. Postnatal maturation of GABAergic modulation of sensory inputs onto lateral amygdala principal neurons: development of sensory input inhibition in mouse lateral amygdala. *J Physiol* 2015;**593**:4387-409.
31. Ehrlich DE, Ryan SJ, Hazra R, Guo J-D, Rainnie DG. Postnatal maturation of GABAergic transmission in the rat basolateral amygdala. *J Neurophysiol* 2013;**110**:926-41.
32. Magee JC. Dendritic integration of excitatory synaptic input. *Nat Rev Neurosci* 2000;**1**:181-90.
33. Sosulina L, Meis S, Seifert G, Steinhäuser C, Pape H-C. Classification of projection neurons and interneurons in the rat lateral amygdala based upon cluster analysis. *Mol Cell Neurosci* 2006;**33**:57-67.
34. Isaeva EV, Sidorenko VG, Fedulova SA, Veselovskii NS. Evoked inhibitory postsynaptic currents in the dynamics of development of cultured hippocampal neurons of rats. *Neurophysiology* 1999;**31**:304-9.
35. Lin Y-C, Huang Z-H, Jan I-S, Yeh C-C, Wu H-J, Chou Y-C, et al. Development of excitatory synapses in cultured neurons dissociated from the cortices of rat embryos and rat pups at birth. *J Neurosci Res* 2002;**67**:484-93.
36. Chareyron LJ, Lavenex PB, Lavenex P. Postnatal development of the amygdala: a stereological study in rats. *J Comp Neurol* 2012;**520**:3745-63.
37. Collier AC, Mast J, Meyer DR, Jacobs C-E. Approach-avoidance conflict in preweanling rats: a developmental study. *Anim Learn Behav* 1979;**7**:514-20.
38. Chen SWC. The role of the amygdala and olfaction in unconditioned fear in developing rats. *J Neurosci* 2006;**26**:233-40.
39. Raineki C, Shionoya K, Sander K, Sullivan RM. Ontogeny of odor-LiCl vs. odor-shock learning: similar behaviors but divergent ages of functional amygdala emergence. *Learn Mem* 2009;**16**:114-21.
40. Shionoya K, Moriceau S, Lunday L, Miner C, Roth TL, Sullivan RM. Development switch in neural circuitry underlying odor-malaise learning. *Learn Mem* 2006;**13**:801-8.
41. Mahan AL, Ressler KJ. Fear conditioning, synaptic plasticity and the amygdala: implications for posttraumatic stress disorder. *Trends Neurosci* 2012;**35**:24-35.
42. Smerin S, Chen A, Li H. Neurophysiology of aggression in posttraumatic stress disorder. *J Psychiatry* 2016;**19**.